



Promoted activity of nitrogen-doped activated carbon as a highly efficient oxygen reduction catalyst in microbial fuel cells

Yuan Liu^{1,2} · Zhi-Mei Liu^{1,2}

Received: 3 August 2018 / Accepted: 7 October 2018 / Published online: 15 October 2018
© Springer Nature B.V. 2018

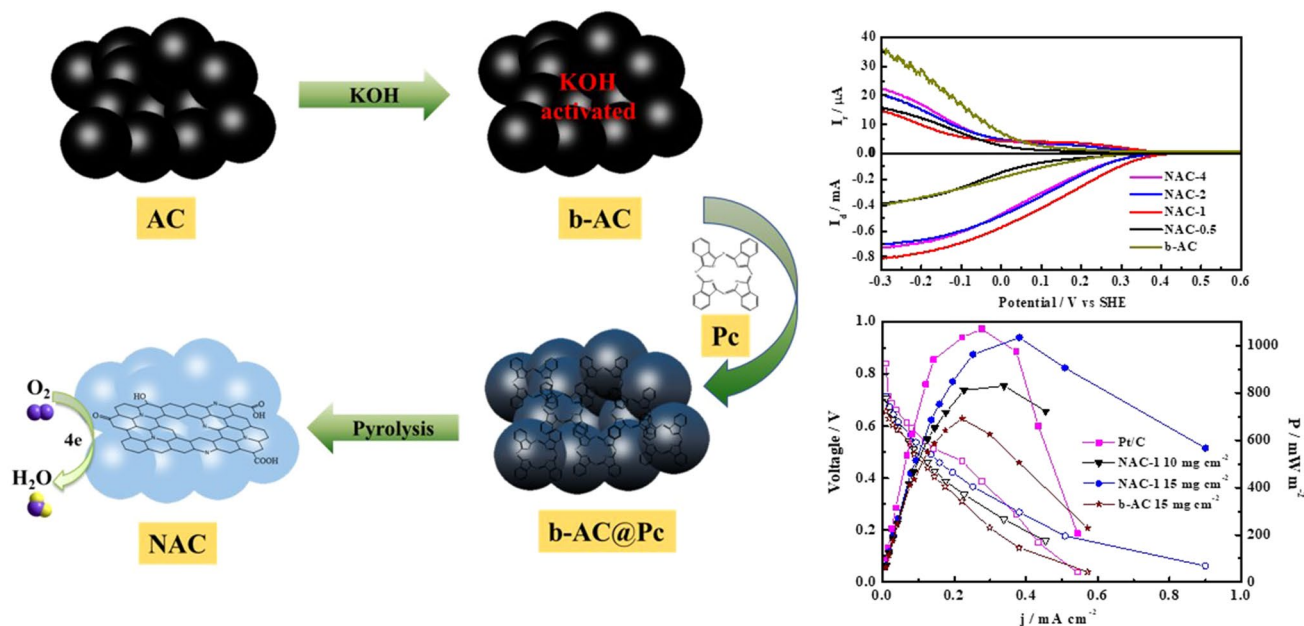
Abstract

Despite the wide application of activated carbon (AC) as cathode electrocatalyst in microbial fuel cell (MFC), the enhancement of its catalytic activity is crucial to reduce its high loading on air-cathode. Herein, we synthesize nitrogen-doped activated carbon (NAC) by pyrolyzing phthalocyanine (Pc) adsorbed on AC to develop an efficient oxygen reduction reaction (ORR) electrocatalyst. The optimized mass ratio of AC to Pc improves the crystalline structure and porous structure of the NAC. Elemental analysis indicates that this material contains appropriate content of pyrrolic and pyridinic types of nitrogen and oxygen species. The NAC shows an ORR onset potential of 0.468 V (vs. Standard hydrogen electrode), an electron transfer number of 3.90, and high electrochemically accessible surface area, thereby illustrating enhanced electrocatalytic activity in the neutral medium relative to alkali-treated activated carbon (b-AC) and commercial platinum catalyst. Owing to the high activity, a small amount of NAC with a loading of 15 mg cm^{-2} on the air-cathode of MFC is sufficient to achieve the maximum power density of $1026.07 \pm 10.83 \text{ mW m}^{-2}$, which is higher than that of b-AC and comparable to platinum catalyst. The reduced loading of NAC indicates that the material can be used as cathode electrocatalyst for the ongoing effort to scale up MFC in the future.

Electronic supplementary material The online version of this article (<https://doi.org/10.1007/s10800-018-1263-6>) contains supplementary material, which is available to authorized users.

Extended author information available on the last page of the article

Graphical abstract



Keywords Activated carbon · Phthalocyanine · Nitrogen-doping · Microbial fuel cell · Oxygen reduction reaction

Abbreviations

AC	Activated carbon
BET	Brunauer–Emmett–Teller
BJH	Barrett–Joyner–Halenda
CE	Coulombic efficiency
COD	Chemical oxygen demand
CV	Cyclic voltammetry
ECSA	Electrochemical accessible surface area
LSV	Linear sweep voltammetry
MFC	Microbial fuel cell
MPD	Maximum power density
NAC	Nitrogen-doped activated carbon
OCV	Open-circuit voltage
ORR	Oxygen reduction reaction
PBS	Phosphate-buffered saline
Pc	Phthalocyanine
PGMs	Platinum group metals
RRDE	Rotating ring-disk electrode
SEM	Scanning electron microscopy
SHE	Standard hydrogen electrode
XPS	X-ray photoelectron spectroscopy
XRD	X-ray diffraction
%H ₂ O ₂	Yield percentage of H ₂ O ₂ (%)
j_0	Exchange current density (mA cm ⁻²)
n	Electron transfer number
η	Overpotential (mV)

1 Introduction

Microbial fuel cell (MFC) is a promising technology that can convert chemical energy in wastewater into electricity via anaerobic biological oxidation at the anode [1–3]. Meanwhile, the oxygen reduction reaction (ORR) at the cathode consumes the electrons released from the anode. Due to the high overpotential and sluggish kinetics of ORR, platinum or platinum group metals (PGMs) had to be widely selected in early studies. However, the high cost, poor stability in long-term operation, and sensitivity to being poisoned by various chemicals of PGMs hinder the large-scale production and further commercialization of MFCs [4–6]. Therefore, it forces us to search or develop cost-effective, sustainable, and highly active alternative ORR catalysts [7–10].

Logan and co-workers found that inexpensive and easily accessible activated carbon (AC) is an effective cathode catalyst in MFC [11]; since then, AC has attracted increasing attention [12–15]. Owing to the high surface area and good porosity of AC, MFCs with AC-based cathode outperform maximum power density of those obtained by Pt/C cathode [16, 17]. The AC-based cathode also shows a better long-term stability than Pt/C cathode [18, 19]. However, the AC-based MFCs often require a high AC loading on air-cathode to achieve desirable power generation because of the poor electrical conductivity and weak ORR kinetics of bare AC [20–22]. High loading undoubtedly

results in a thick catalyst layer that blocks mass transport [23]. Therefore, considerable efforts for improving the catalytic activity of AC and lowering its loading on air-cathode have been made.

The incorporation of highly conductive materials (e.g., carbon black, carbon nanotubes, and metal nanoparticles) efficiently improves the electrical property of AC [20, 22, 24]. Moreover, the addition of metal nanoparticles, especially silver nanoparticles, can inhibit biofilm growth on an AC cathode [24]. Conductive metal oxides, such as CoO and Cu₂O, can also serve as active sites to enhance the ORR activity of AC [25, 26]. Acid and alkaline pretreatments are simple and effective methods that improve the catalytic performance of AC [27–29]. Chemical treatment can introduce oxygen-containing functional groups on the AC surface, which can reduce the energy barriers of oxygen adsorption and provide ORR sites. Heteroatom-doping (e.g., N, S, and P) also enhances the ORR activity of AC. On bare AC, ORR occurs through a two-electron transfer pathway [30]. Heteroatom-doped AC can adjust the ORR into a four-electron transfer pathway [29, 31–33]. Heteroatom-doping can increase the surface area or form associated functional groups on an AC surface, thereby improving the ORR activity of AC. The maximum power density of MFCs can be significantly increased by 28–107% by using heteroatom-doped AC as a cathode catalyst [33]. The co-doping of N and transition metals (i.e., Fe or Co) into AC can significantly improve ORR activity. This improvement is facilitated by the immobilization of an M–N–C co-catalyst, in which M–N_x serves as an active site to drive ORR via a four-electron transfer pathway [21, 34–36]. The enhanced ORR activity of heteroatom-doped AC can be expected to reduce catalyst loading on an air-cathode.

Compounds with high nitrogen content, such as cyanamide, melamine, and urea, are crucial to the successful doping of nitrogen into AC. Due to the poor interaction between AC and nitrogen source, high mass ratio of nitrogen source to AC (i.e., 5:1) was required to achieve desirable ORR activity [31]. Phthalocyanine (Pc) is a macrocyclic compound that has a high nitrogen content and can thus be selected as a nitrogen source for the synthesis of non-noble metal ORR catalysts. Its metallic derivatives, such as Fe(II) or Co(II)–Pc, are frequently selected for the synthesis of MN₄-modified ORR catalysts [37–41]. As far as we know, however, the single Pc monomer is barely used as nitrogen precursor for the synthesis of nitrogen-doped carbon materials. The molecules of Pc have planar structure, which facilitates the adsorption of Pc on carbon materials via strong interaction. Consequently, nitrogen can be readily doped into AC, and a high nitrogen content is expected. Moreover, the mass ratio of Pc to AC is also expected to be lowered. Therefore, nitrogen-doped AC (NAC) is expected to be synthesized by using Pc as nitrogen source.

The present work reports a systematic synthesis of NAC by using Pc as nitrogen source and AC as support. The physical and chemical properties of NAC were systematically analyzed by using scanning electron microscopy (SEM), X-ray diffraction (XRD), Raman spectroscopy, Brunauer–Emmett–Teller (BET) adsorption, and X-ray photoelectron spectroscopy (XPS). The electrocatalytic activity of ORR was investigated with a rotating ring-disk electrode (RRDE) apparatus. NAC was also applied as cathode electrocatalyst in dual-chamber air-cathode MFC to estimate its feasibility for power generation.

2 Materials and methods

2.1 Chemicals

Pc was purchased from Tokyo Chemical Industry Co., Ltd. and used without further purification. A peat-based AC (Norit SX) was purchased from Sigma-Aldrich, pretreated in 3 M of KOH at 85 °C for 6 h, and denoted as b-AC. Analytical grade chemicals were used for all experiments, and no further purification was performed. Ultrapure water (18.2 MΩ cm⁻¹ at 25 °C, total organic carbon < 5 ppb) was produced from Millipore water system (Synergy UV).

2.2 Catalyst synthesis

A typical synthesis route can be summarized as follows: 50 mg of alkali-treated activated carbon (b-AC) was dispersed in 50 mL of ethanol via 30-min sonication. Then, 12.5, 25, 50, or 100 mg of Pc was added into the solution with further sonication for another 30 min. The solvent was slowly removed in an oven at 65 °C for overnight. Subsequently, the obtained powder coated with Pc was ground and heat-treated in argon atmosphere by heating at 1000 °C at a rate of 5 °C min⁻¹ and holding for 1 h. Finally, the sample was washed with deionized water until the filtrate was neutral and then dried for overnight via lyophilization before further measurements. The as-prepared materials were named as NAC-*x* (*x* represents the mass ratio of AC to Pc; *x* = 0.5, 1, 2, 4).

2.3 Material characterizations

The morphology of NAC electrocatalysts was observed using an SEM system (JEOL, JSM-7800F). The crystal-line structure of NAC-*x* was analyzed using a powder XRD (X'Pert³ powder diffractometer) with Cu–Kα radiation source ($\lambda = 1.54056 \text{ \AA}$). The Raman spectra were obtained on a laser confocal Raman spectrometer (Renishaw inVia Reflex) by using a 532 nm wavelength laser. The nitrogen adsorption–desorption isotherms were obtained at 77 K by

using BELSORP-max instrument. The surface area of NAC-x was calculated by BET method. The pore size distribution was calculated according to Barrett–Joyner–Halenda (BJH) model, and the t-plot method was utilized to extract the microporous surface area and volume. XPS measurements were conducted using an ESCALAB 250Xi spectrometer (Thermo Electron, UK) with an Al-K α X-ray source.

2.4 Electrochemical measurements

All the electrochemical measurements of the electrocatalysts were performed on a 760E workstation (CH Instrument, USA) equipped with an MSR electrode rotator (Pine Instrument Co., USA). A conventional three-electrode cell was used. Here, Ag/AgCl electrode (saturated KCl, 0.197 V versus Standard hydrogen electrode [SHE]) and Pt mesh were used as the reference and counter electrodes, respectively. A 5.0-mm diameter glassy carbon disk (Pine Instrument Co., USA) with a Pt ring was used in the RRDE experiments.

For the electrochemical measurements, 1.0 mg mL⁻¹ catalyst ink was prepared by ultrasonically dispersing 5.0 mg of catalyst in 5.0 mL of ethanol. Approximately 50 μ L of 5 wt% Nafion (DuPont Company) was added to the system, and the resulting mixture was ultrasonicated for 30 min. Then, 19.6 μ L of the ink was pipetted onto the glassy carbon disk, which was initially polished using 0.05 μ m alumina slurry. For comparison, a commercial Pt/C catalyst containing 20 wt% Pt supported on carbon black (Johnson Matthey Corp., HISPEC 3000) was used, and the ink was prepared by using the same procedures described above. All catalyst loadings on the glassy carbon disk were 100 μ g cm⁻².

All RRDE tests were conducted at 25 °C in N₂- or O₂-saturated 0.1 M phosphate-buffered saline (PBS, pH 7.0) aqueous solution. The cyclic voltammetry (CV) curves of the electrocatalysts were recorded at a potential sweep speed of 50 mV s⁻¹. The ORR polarization curves of RRDE were obtained at a potential sweep rate of 5 mV s⁻¹ with a potential range from 0.6 to -0.6 V (vs. Ag/AgCl) and rotating speed from 400 to 2400 rpm, with the ring potential fixed at 0.6 V (vs. Ag/AgCl). The yield percentage of H₂O₂ and the electron transfer number (n) were determined by the following equations:

$$\%H_2O_2 = 200 \times \frac{I_r/N}{I_d + I_r/N} \quad (1)$$

$$n = 4 \times \frac{I_d}{I_d + I_r/N} \quad (2)$$

where I_d is the disk current; I_r is the ring current, and N is the current collection efficiency of the Pt ring. N is 0.21 \pm 0.01 from the reduction of K₃Fe(CN)₆.

The Tafel plot was recorded by sweeping the overpotential from -100 to 100 mV versus the open-circuit potential at 1 mV s⁻¹, from which the exchange current density (j_0) was calculated [16]. The electrochemical accessible surface area (ECSA) of the electrocatalysts was also estimated by using CV, which was conducted in 5 mM aqueous potassium ferricyanide aqueous containing 0.1 M LiClO₄ as the supporting electrolyte [42]. ECSA was calculated using the following equations [43]:

$$i_p = (2.69 \times 10^5) n^{3/2} A D_0^{1/2} C_0^* \nu^{1/2} \quad (3)$$

where i_p (A) is the peak current; n is the number of electrons transferred during the reduction of Fe(CN)₆³⁻ (assumed as 1 for this case); A (cm²) is the ECSA; D_0 is the diffusion coefficient of Fe(CN)₆³⁻ (0.7 \times 10⁻⁵ cm² s⁻¹ in aqueous solution); C_0^* is the bulk concentration of Fe(CN)₆³⁻ (5 \times 10⁻⁶ mol mL⁻¹), and ν (in V s⁻¹) is the scan rate. ECSA can be evaluated from the slope of i_p versus $\nu^{1/2}$ plot [43, 44].

2.5 MFC setup and measurement

MFCs were composed of dual-chamber cubic-shaped reactors. Each chamber was 2.0-cm in length and 3.0-cm in diameter. The anode and cathode chambers were separated by a proton-exchange membrane (Nafion® 117, DuPont Company) after pretreatment [45]. The carbon brush (2.0 cm in length and 2.0 cm in diameter) was pretreated using ammonia gas before being used as the anode. An air-cathode made from waterproof carbon cloth containing poly(dimethylsiloxane) as a diffusion layer was fabricated as described in a previous study [46]. A certain amount of NAC and 2.5 mg cm⁻² of 20 wt% Pt/C catalysts were sprayed on the water-facing side of the carbon cloth. The anodic chamber was inoculated with a solution obtained from MFC that has been operating for over a year in the laboratory. The anodic chamber was filled with a mixture of 0.1 M PBS (pH 7.0) containing 1.0 g L⁻¹ sodium acetate, 0.13 g L⁻¹ KCl, 0.31 g L⁻¹ NH₄Cl, 12.5 mL L⁻¹ mineral solution, and 5 mL L⁻¹ vitamin solution [47]. The anodic feed solution was purged with N₂ before inoculation to maintain an anaerobic condition. The cathodic chamber was filled with the same mixture media but without sodium acetate, minerals, and vitamin solutions. The anode and cathode were connected with a 1000 Ω external resistor by using titanium wire, and all exposed metal surfaces were sealed with non-conductive epoxy. All the reactors were operated in a fed-batch mode at 30 \pm 1 °C. The feed solution was replaced once the cell voltage decreased to below 20 mV, which was noted as a complete cycle of electricity generation.

The cell voltage across the external resistor was measured using a multimeter equipped with a data acquisition

system (Advantech, PCI-1747U). The maximum power density (MPD) of the MFC was obtained from the polarization curves by varying the resistance of the external resistor from an open-circuit voltage (OCV) to 10 Ω as the performance of MFC approach steady-state conditions. Data were recorded as < 1 mV variation in voltage. All the experiments were conducted twice at room temperature (30 ± 1 °C). Power density was calculated based on the anode area, as shown as follows:

$$p = \frac{E_{\text{cell}}^2}{A_{\text{cat}} R_{\text{ext}}} \quad (4)$$

where E_{cell} is the cell voltage (mV); R_{ext} is the external resistance (Ω), and A_{cat} is the cathode project area (m^2). The coulombic efficiency (CE) over time (t) was calculated using Eq. (2), as shown as follows:

$$\varepsilon_{\text{CE}} = \frac{8 \int_0^t Idt}{FV_{\text{An}} \Delta_{\text{COD}}} \quad (5)$$

where V_{An} (L) is the volume of the liquid in the anode chamber, and Δ_{COD} is the change in chemical oxygen demand (COD) over t .

3 Results and discussion

3.1 Characterization of NAC-x catalysts

The SEM images of b-AC and NAC-1 are shown in Fig. 1a, b, from which no significant difference in morphology was observed. Thus, nitrogen-doping did not affect the morphology of the catalysts. NAC-1 was further characterized by taking the elemental-mapping images of carbon, oxygen, and nitrogen (Fig. 1c). The nitrogen elements were uniformly dispersed on the AC surface, which indicate that the present method was efficient for the uniform incorporation of nitrogen.

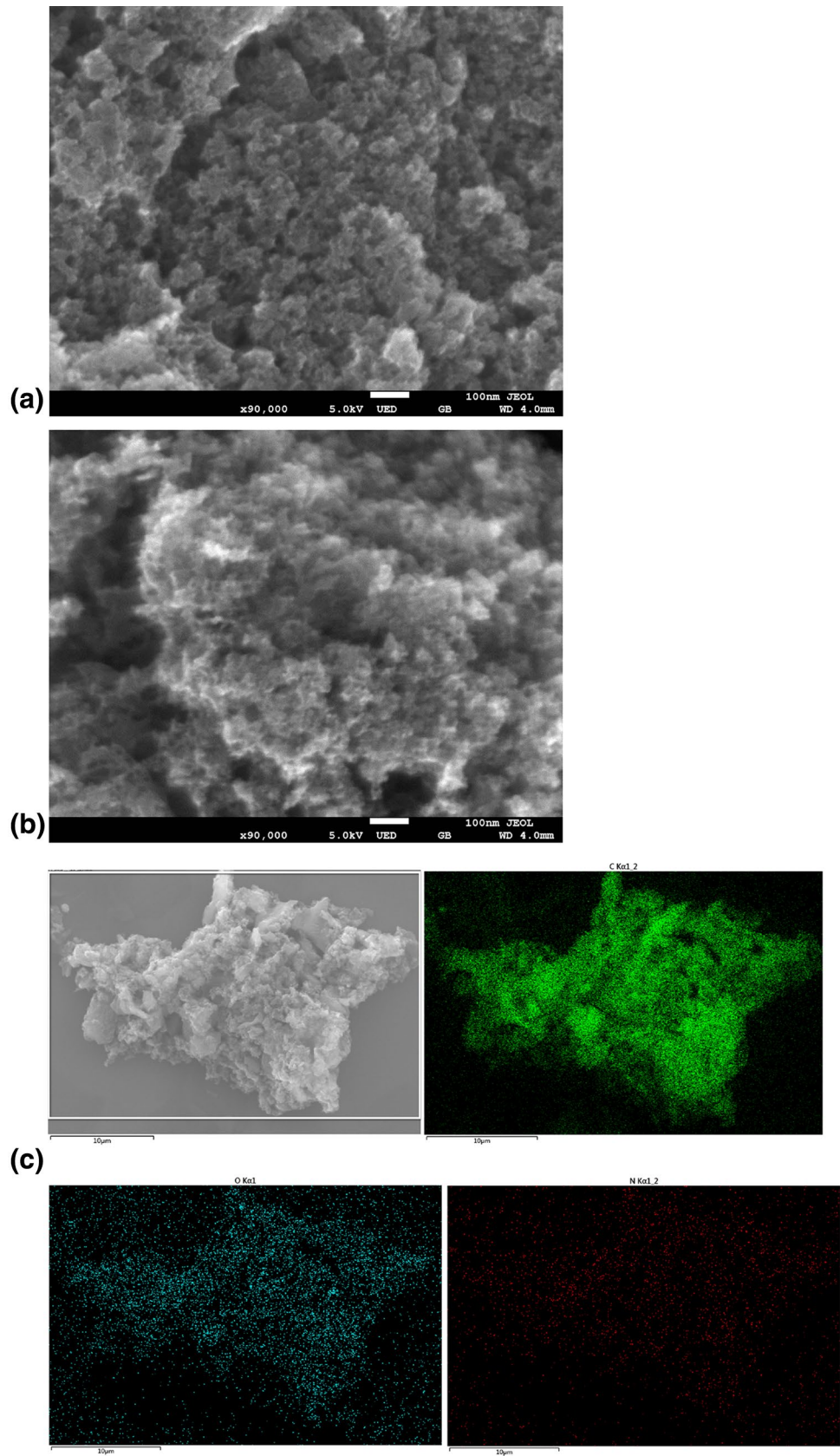
To further investigate the crystalline structure of AC-based catalysts, XRD and Raman analyses were conducted, and the corresponding results are presented in Fig. 2. The XRD patterns in Fig. 2a show the appearance of broad peaks at 23° and 43° , which corresponded to the (002) and (100) carbon, respectively. The results also indicated the existence of graphitic carbon structure. The intensities of the (100) peak of NAC-x catalysts were stronger than those of b-AC, which indicated a high graphitization degree. This phenomenon was also confirmed by the results of Raman analysis. As shown in Fig. 2b, all the Raman spectra of the catalysts displayed two wide peaks at $\sim 1327 \text{ cm}^{-1}$ (D-band) and $\sim 1594 \text{ cm}^{-1}$ (G-band). The intensity ratio of D-band to G-band ($I_{\text{D}}/I_{\text{G}}$), which represented the average graphitization

degree, was calculated and listed in Table 1. The $I_{\text{D}}/I_{\text{G}}$ values of NAC-x decreased compared with b-AC, which demonstrated the increase in the average graphitization degree. Moreover, both NAC-1 and NAC-2 possessed lower $I_{\text{D}}/I_{\text{G}}$ value than the other samples, which indicated that these catalysts with moderate nitrogen doping possessed higher graphitization degree and superior electrical conductivity. The result also indicated that excessive and insufficient Pc dosage caused lower graphitization degree for NAC-0.5 and NAC-4.

The surface area and porosity of AC-based catalysts were examined by nitrogen adsorption–desorption measurements (Fig. 3a). Similar isotherms of type IV with an obvious hysteresis loop were observed at a medium relative pressure, which indicated the existence of mesopores. Furthermore, the rapid increase at low relative pressure indicated the presence of micropores [8, 48]. As shown in Fig. 3b, the BJH pore size distribution curves of the AC-based catalysts confirmed the abundance mesopores with diameter of < 10 nm. Table 1 summarizes the textural parameters of the AC-based catalysts derived from the nitrogen isotherms. All the NAC-x catalysts exhibited reduced BET surface area and pore volume compared with b-AC, whereas the mean pore size of all samples did not show obvious change. Despite these observations, NAC-1 possessed a BET surface area of $796.58 \text{ m}^2 \text{ g}^{-1}$ and a total pore volume of $0.561 \text{ cm}^3 \text{ g}^{-1}$. The decreased BET surface area and pore volume were likely due to the occupancy of partial pores of AC by the deposition of Pc during pyrolysis [49]. It could also be attributed to the pore shrinkage and blocking of the pore space by some surface functionalities at high temperature [32]. Moreover, the BET surface area and pore volume of NAC-0.5 significantly decreased, which indicated that a high Pc dosage might be contrary to the electrocatalytic activity of as-prepared catalyst. Despite the reduced BET surface area and pore volume, the abundant micropores of NAC-x catalysts could provide sufficient activity sites for ORR, which enhanced the catalytic activity [50]. Moreover, sufficient mesopores could guarantee the mass transport on the surface of NAC-x catalysts to enable efficient ORR [51]. In addition, the balance between mass transport and active sites could play more important role in ORR activity than single surface area or porosity [52].

XPS measurements were performed to probe the chemical composition of AC-based catalysts. The survey spectra in Fig. 4a indicated the presence of C 1s, N 1s, and O 1s for all NAC-x catalysts, and the textural parameters are summarized in Table 1. Compared with b-AC, the N content for all NAC-x samples significantly increased, which demonstrated the successful doping of nitrogen by using Pc as a nitrogen source. As shown in Table 1, the N content of NAC-x was highly dependent on the Pc dosage, that is, the NAC-0.5 possessed the highest N content (2.98 at.%), whereas NAC-4

Fig. 1 SEM images of **a** b-AC, **b** NAC-1, and **c** corresponding elemental mapping images for C, O, and N



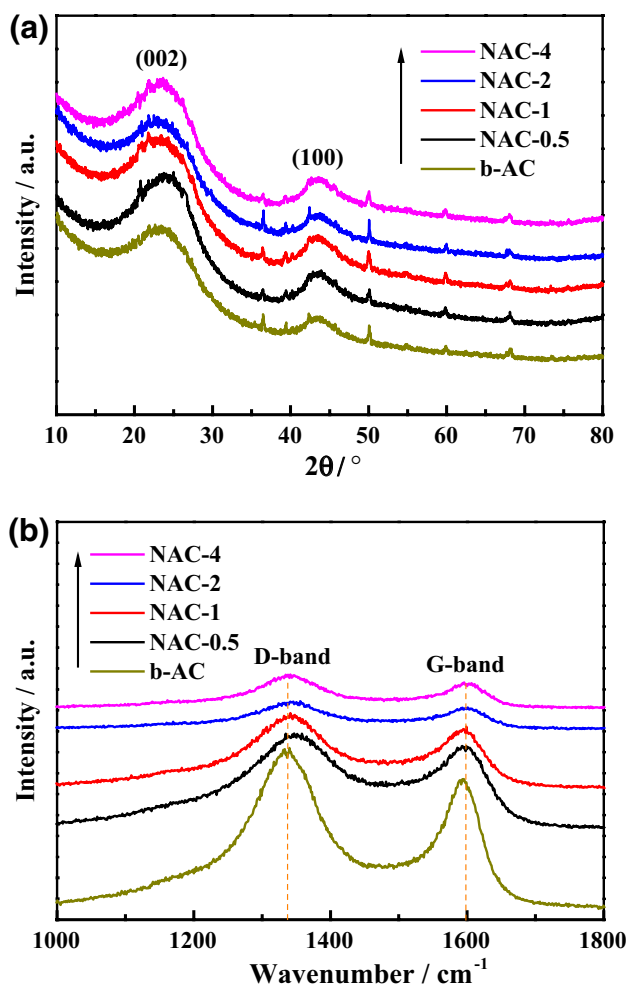


Fig. 2 XRD (a) and Raman (b) spectra of AC-based electrocatalysts

possessed the lowest N content (1.40 at.%). The high resolution of N 1s spectrum (Fig. 4b and S1) was fitted into three bands at ~ 398.5 , 399.8 , and 401.5 eV, which corresponded to pyridinic, pyrrolic, and graphitic nitrogen, respectively [53, 54]. Different types of N species play different roles in ORR. Pyridinic and pyrrolic N can reduce the adsorption energy of O_2 , which result in ORR readily on N-doped carbon materials. Graphitic N can reduce O_2 to H_2O_2 via adsorbed OOH intermediates through a two-electron pathway, whereas pyridinic and pyrrolic N species may convert the ORR mechanism from a two-electron to a four-electron dominating process [53, 55, 56]. As an alkaline group, the pyridinic N participates in ORR directly and/or indirectly. In the direct way, pyridinic N provides ORR active sites by enhancing the adoption of proton from HPO_4^{2-} and $H_2PO_4^-$ in PBS through charge neutralization effect [57]. In the indirect way, the carbon atoms next to pyridinic N with Lewis basicity might be the active sites for ORR via enhanced adsorption of oxygen [58].

In addition, two main peaks of C1s and O1s were identified. From Fig. 4c and S2, the C1s were deconvoluted into four species, namely, graphitized carbon (284.6 eV) and the carbon in ether or phenol groups (286.0–286.3 eV), the carbon in carbonyl groups (287.3–287.6 eV), and the carbon in carboxyl or esters groups (288.8–289.1 eV) [59]. The O1s could be deconvoluted into four peaks at 531.2, 532.4, 533.3, and 534.3 eV (Fig. S3), which were correspond to C=O, C–O, RCOOR, and COOH, respectively [59]. Except for b-AC (Fig. S4a), the contents of graphitized carbon for all samples were affected by the dosage of Pc. Excessive or insufficient Pc dosage resulted in a low content of graphitized carbon of NAC-0.5 or NAC-4. Moreover, the tendency of the contents of graphitized carbon agreed with the tendency of I_D/I_G values. In our

Table 1 Characteristics and textural parameters of AC-based electrocatalysts

	b-AC	NAC-0.5	NAC-1	NAC-2	NAC-4
I_D/I_G	1.22	1.07	1.03	1.03	1.08
$S_{BET}/m^2 g^{-1}$	1067.6	459.14	796.58	812.86	846.15
$S_{micropore}/m^2 g^{-1}$	839.55	347.70	608.08	598.89	618.10
$S_{mesopore}/m^2 g^{-1}$	228.05	111.44	188.50	213.97	228.05
Total $V_{pore}/cm^3 g^{-1}$	0.774	0.298	0.561	0.633	0.666
$V_{micropore}/cm^3 g^{-1}$	0.376	0.150	0.265	0.254	0.268
$V_{mesopore}/cm^3 g^{-1}$	0.398	0.148	0.296	0.379	0.398
Mean pore diameter/nm	2.90	2.60	2.82	3.12	3.15
C1s/at. %	92.69	89.55	93.39	93.50	93.69
N1s/at. %	0.56	2.98	1.61	1.57	1.40
Pyridinic N	–	0.67 (22.5%) ^a	0.37 (23.0%)	0.32 (20.4%)	0.17 (12.2%)
Pyrrolic N	–	0.88 (29.5%)	0.57 (35.4%)	0.61 (38.8%)	0.44 (31.4%)
Graphitic N	–	1.43 (48.0%)	0.67 (41.6%)	0.64 (40.8%)	0.79 (56.4%)
O1s/at. %	6.75	7.47	5.00	4.93	4.91

^aThe relative percentage of each N functionality among the N content on the AC surface

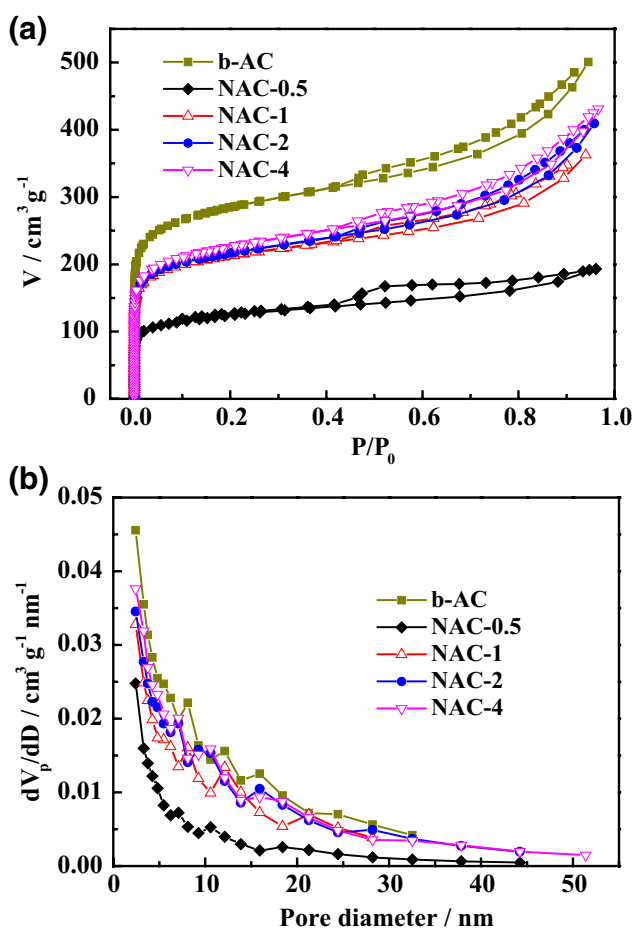


Fig. 3 N_2 adsorption and desorption isotherms (a) and pore size distribution curves (b) of AC-based electrocatalysts

previous studies, oxygen-containing functional groups could enhance the ORR activity of metal-free catalysts [8, 9, 60]. However, excessive oxygen content in AC could decrease its electrochemical performance [61]. Therefore, high oxygen content (Table 1 and Fig. S4b) might decrease the ORR activity of b-AC and NAC-0.5. The contents of C=O, C–O, and RCOOR were almost positively correlated to the electrochemical performance of catalysts [6, 62]. A strong proton affinity to non-acid groups (i.e., C=O and C–O) would favor O_2 adsorption [27, 63]. Moreover, the ester group (RCOOR) served as an active site for pseudocapacitance [64]. Thus, the high amount of C=O, C–O, and RCOOR of NAC-1 and NAC-2 could facilitate to enhance their ORR activities. In addition, not all functional groups with oxygen are beneficial for ORR. The presence of strong acid functional groups (e.g., COOH) causes less stability, and excessive COOH would inhibit the effect of proton, which diminishes the ORR activity of ACs [30, 65]. As a result, an excessive amount of COOH could lower the ORR activity of NAC-4.

3.2 Electrocatalytic activity toward ORR

CV and RRDE tests were performed to evaluate the electrocatalytic activity of NAC-*x* catalysts. Figure 5a and S5 demonstrates the results of CV performed with and without O_2 in 0.1 M PBS solution. In comparison with the CV performed without O_2 , evident ORR peaks were observed in the potential range of -0.1 V to 0.2 V (vs. SHE) in the presence of O_2 for all NAC-*x* catalysts. The ORR peak of NAC-1 displayed a more positive potential compared with its counterparts, whilst the NAC-0.5 with the highest Pc dosage showed the most negatively shifted ORR peak potential. To further explore the ORR mechanism, RRDE linear sweep voltammetry (LSV) was conducted at various rotating rates, and the corresponding results are depicted in Fig. 5b and S6. The current densities were significantly enhanced by increasing rotating rate for all samples, indicating a fast oxygen flux from the bulk solution to the electrode surface under high rotating rate [66]. The incorporation of nitrogen into AC could enhance the current densities at all rotating rate, although apparent discrepancy compared with Pt/C was still observed.

Figure 5c compares the RRDE results at a rotating rate of 1600 rpm for all AC-based catalysts. One can see that as the potential was negatively swept, the non-zero current started to emerge, indicating oxygen reduction catalyzed by these carbon materials. On the basis of the LSV curves, the onset potentials for all samples are summarized and listed in Table 2. After nitrogen-doping, the onset potential of NAC-*x* catalysts showed a prominently positive shift from 0.358 V (vs. SHE) of b-AC to 0.435 V (vs. SHE) of NAC-1. A lower positive shift of onset potential was observed for catalysts with excessive (0.391 V for NAC-0.5) or insufficient (0.396 V for NAC-4) nitrogen-doping. Except for NAC-0.5, the ORR current densities were considerably increased, indicating the presence of more active sites and improved mass transport of the nitrogen-doped catalysts. In comparison with previous studies (Table S1), the AC modified with Pc in this work showed more positively shifted onset potential of ORR [17, 31, 33, 48]. It is suggested that Pc was a good alternative nitrogen source to synthesize nitrogen-doped carbon catalysts.

The corresponding H_2O_2 yield and *n* values were calculated based on the RRDE tests and are displayed in Fig. 5d. All the NAC-*x* catalysts showed an improved ORR activity in terms of low H_2O_2 yield and high *n* value after nitrogen-doping. With the calculated *n* of 3.18, b-AC exhibited a two- and four-electron mixed ORR pathways [67]. As listed in Table 2, the average *n* values were 3.57, 3.70, 3.72, and 3.80 for NAC-0.5, NAC-4, NAC-2, and NAC-1, respectively. The results illustrated that NAC-1 proceeded through a dominant four-electron reaction pathway, which could provide a positive electrode potential. The *n* value of NAC-1 was

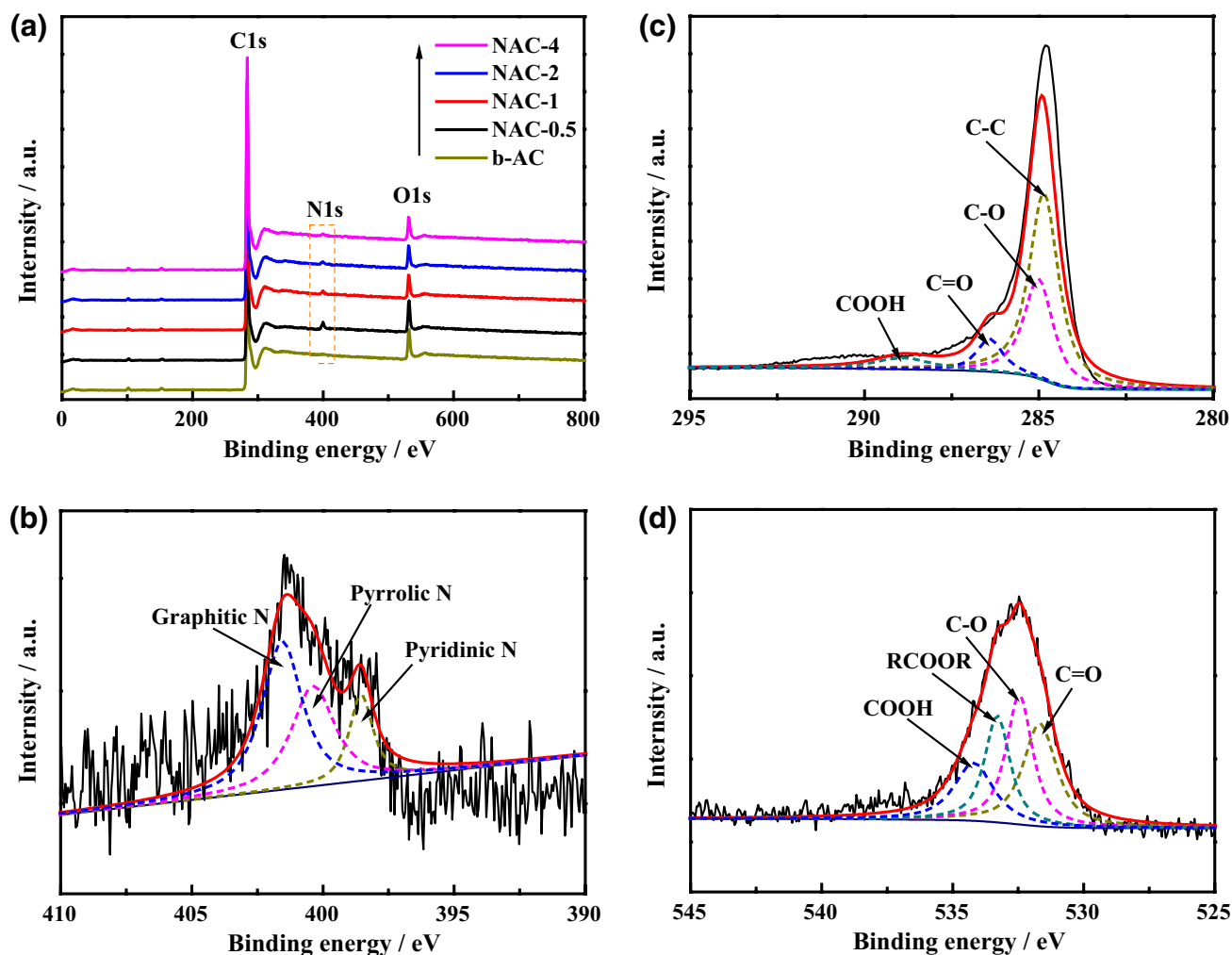


Fig. 4 XPS survey of AC-based electrocatalysts (a) and high resolution of N1s (b), C1s (c), and O1s (d) of NAC-1

much higher than those nitrogen-doped carbon materials previously reported [33, 48]. The trend of n values was in accordance with the result of onset potential. Meanwhile, the H_2O_2 yield dramatically decreased after nitrogen-doping compared with b-AC. With respect to NAC-1, the average H_2O_2 yield was below 10%. The results indicated that Pc was an efficient precursor for the synthesis of NAC. NAC-1 with high n value and positive onset potential was supposed to facilitate the power generation of MFC. NAC-0.5 possessed a lower electron-transfer number than the other NAC catalysts despite having high nitrogen content. The results suggested that an appropriate chemical composition plays a significant role in the enhancement of electrocatalytic activity of catalysts.

The Tafel plots of all AC-based catalysts is shown in Fig. S7a, and linear fitting from ± 80 to 100 mV versus open-circuit potential was conducted to obtain j_0 [13]. The corresponding values of j_0 are listed in Table 2. The j_0 of NAC-1 was the highest ($2.08 \times 10^{-6} \text{ mA cm}^{-2}$) and was

approximately 5.6%, 8.9%, 35.1%, and 85.7% higher than that of NAC-4, b-AC, NAC-2, and NAC-0.5. This result indicated that the ORR kinetics of NAC-1 was significantly promoted and was supposed to subserve the improvement of MFC power output. ECSA can reflect the actual available surface area for electrochemical reaction. As shown in Fig. S7b, NAC-1 and NAC-2 possessed the highest ECSA. The tendency of ECSA values agreed with the tendency of the current density of LSV. The ECSAs were smaller than those obtained from BET measurement, which was due to the presence of intrinsic resistance, non-flat surface, non-accessible micropores, and variation of oxygen concentration on the surface [42]. The results demonstrated that keeping a balance between the surface area for serving as active sites and porosity for mass transport was of great importance for the enhancement of the electrocatalytic activity of catalysts.

Metal-free catalysts often catalyze the ORR process via indirect four-electron pathway that involves the formation of a large amount of intermediate peroxide [68]. Varying

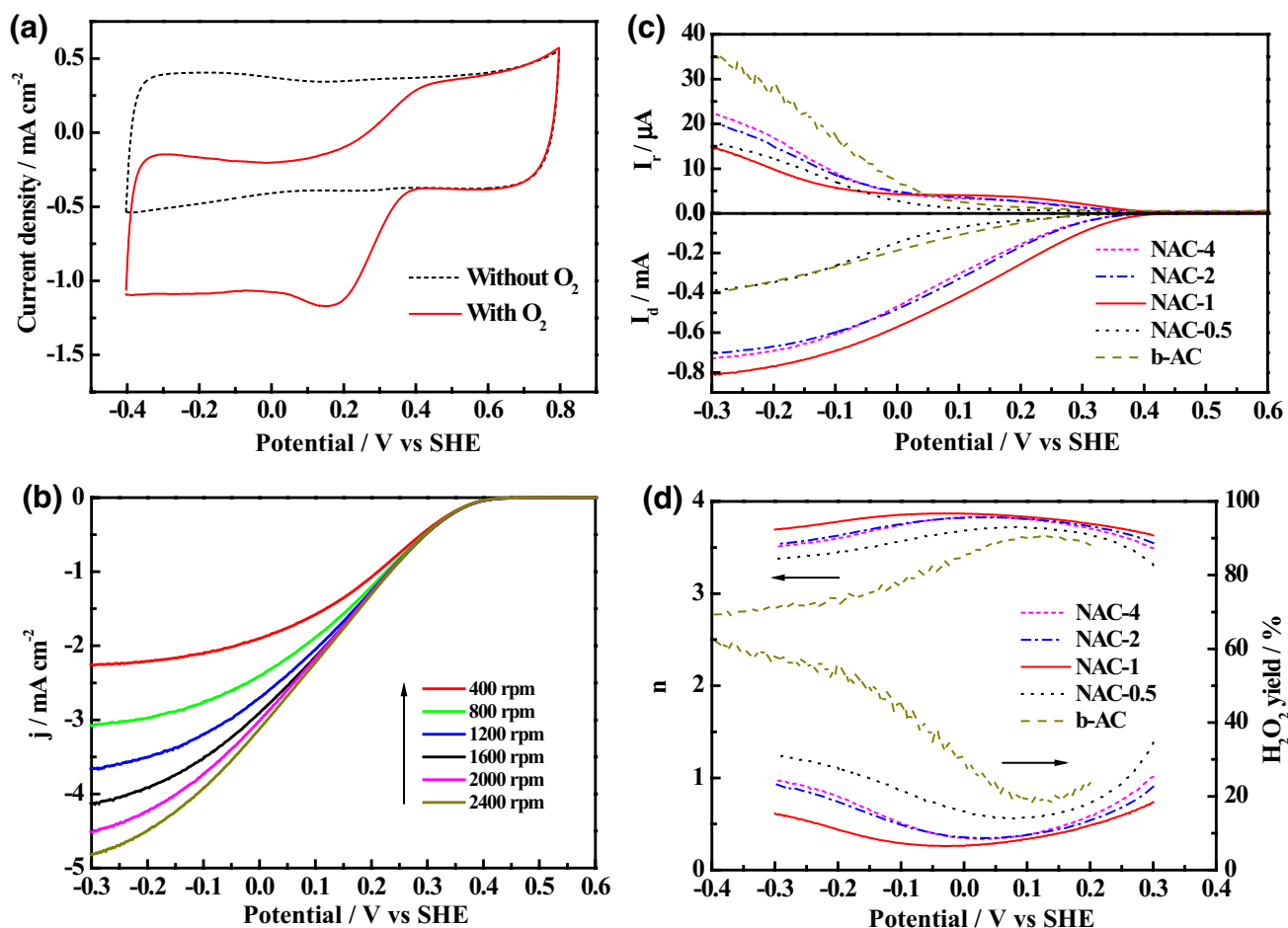


Fig. 5 Cyclic voltammograms (a), polarization curves of ORR at different rotating rates (b) of NAC-1, comparison of current–potential profiles of RRDE tests at 1600 rpm (c) and corresponding H_2O_2 yield and electron transfer number (d) of AC-based electrocatalysts

the thickness of the electrocatalyst layer is an effective method to investigate the mechanism of ORR [69, 70]. Figure 6 displays the results of RRDE tests at different electrocatalyst loadings of NAC-1. As shown in Fig. 6a, the current density increased as the electrocatalyst loading increased from $100 \mu\text{g cm}^{-2}$ to $800 \mu\text{g cm}^{-2}$. As the loading reached $500 \mu\text{g cm}^{-2}$, the current density became close to that of Pt/C. As shown in Fig. 6b, the H_2O_2 yield

and n value exhibited a clear correlation with the electrocatalyst loading on RRDE. The H_2O_2 yield decreased and the n value increased with the increasing electrocatalyst loading. At a loading of $800 \mu\text{g cm}^{-2}$, the n value could reach 3.90 and the average H_2O_2 yield was below 5%, which were close to those of the Pt/C (Table S1). Furthermore, the onset potential was dependent on the electrocatalyst loading. As listed in Table S1, the onset potential increased from 0.435 V to 0.468 V (vs. SHE) as the loading increased from 100 to $800 \mu\text{g cm}^{-2}$. This result could be ascribed to the generated H_2O_2 that could be further reduced to H_2O at other ORR active sites in the thick electrocatalyst layer at a high electrocatalyst loading. In addition, the as-prepared catalyst in this work displayed superior electrochemical properties compared with other chemical-modified ACs reported in previous studies, as shown in Table S1. A small amount of NAC-1 is expected when applied as a cathode electrocatalyst in MFC.

Table 2 Electrochemical properties of AC-based electrocatalysts

Samples	Onset potential/V versus SHE	n	$j_0(10^{-6} \text{ mA cm}^{-2})$	ECSA ($\text{m}^2 \text{ g}^{-1}$)
b-AC	0.358	3.18 ± 0.31	1.91	0.72
NAC-0.5	0.391	3.57 ± 0.12	1.12	0.43
NAC-1	0.435	3.80 ± 0.06	2.08	0.86
NAC-2	0.410	3.72 ± 0.09	1.54	0.86
NAC-4	0.396	3.70 ± 0.11	1.97	0.72

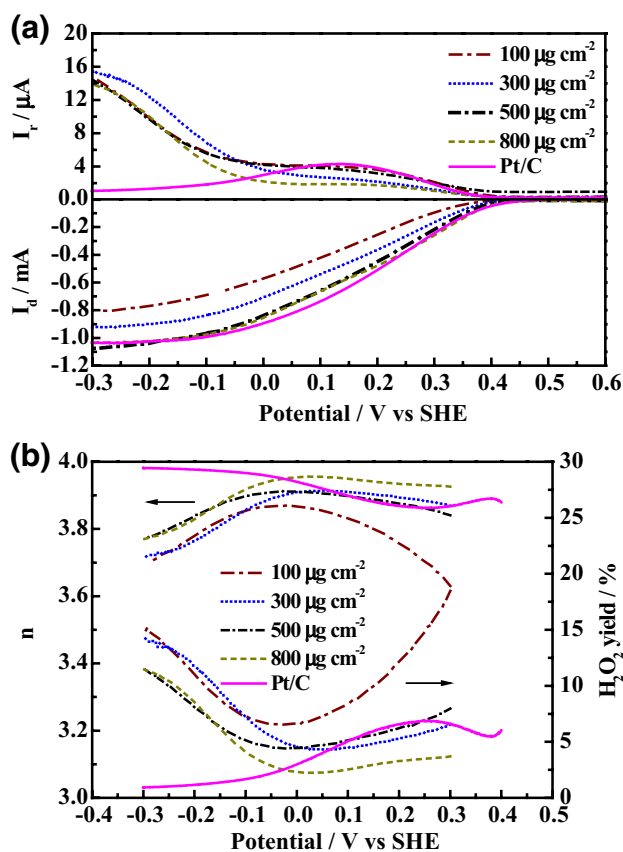


Fig. 6 Comparison of current–potential profiles of RRDE tests (a) and corresponding H_2O_2 yield and electron transfer number (b) at different electrocatalysts loading of NAC-1 and Pt/C

3.3 Application as cathode electrocatalysts in MFC

NAC-1 and b-AC with different loadings were prepared as air-cathodes and equipped into MFCs to investigate their feasibility as alternatives to Pt/C. The voltage output and power generation of different MFCs were compared. Figure 7a shows the voltage output of MFCs equipped with different electrocatalysts. A similar trend in cell voltage variation for each type of MFCs was observed. The cell voltage initially increased to a maximum and then gradually decreased as electricity was generated. As summarized in Table 3, Pt/C-MFC generated the highest maximum voltage (568.85 ± 2.92 mV), followed by 15 mg cm^{-2} of NAC-1 (535.43 ± 1.53 mV), 10 mg cm^{-2} of NAC-1 (514.17 ± 8.25 mV), and 15 mg cm^{-2} of b-AC (506.46 ± 2.36 mV). The order was in accordance with the onset potential of ORR. A more positive onset potential indicated less overpotential and a high cell voltage output. The results implied that nitrogen-doping with Pc as nitrogen source could enhance the ORR activity of AC. With respect to NAC-1, a high catalyst loading could provide additional active sites for ORR and additional channels for

mass transport, resulting in the high voltage output of MFCs. Identical COD removal on all cases implied that the efficiencies of anodic reaction were kept constant in all cells due to the same electrode material and bacterial inoculum. However, the results of CE showed a significant discrepancy among these MFCs. NAC-MFC possessed a higher CE than those of Pt/C and b-AC. This finding indicated that the activity of cathode played an important role in the power generation of MFCs. Moreover, NAC would be a promising cathode electrocatalyst for MFC.

Power generation is one of the most significant evaluation parameters for MFC performance. Figure 7b shows the polarization and power density curves of MFCs, and Table 3 summarizes the corresponding MPD of MFCs equipped with different electrocatalysts. As shown in Fig. 7b, by using 15 mg cm^{-2} of NAC-1, the air-cathode MFC generated an OCV of 0.714 V, which was smaller than Pt/C (0.841 V) but higher than 10 mg cm^{-2} of NAC-1 (0.706 V) and b-AC (0.655 V). The order agreed with that of the onset potential of the electrocatalysts. The power density curves of air-cathode MFC using different electrocatalysts had an MPD order as follows: Pt/C (1065.33 ± 6.29 mW m^{-2}) > 15 mg cm^{-2} of NAC-1 (1026.07 ± 10.83 mW m^{-2}) > 10 mg cm^{-2} of NAC-1 (829.73 ± 9.31 mW m^{-2}) > 15 mg cm^{-2} of b-AC (690.86 ± 12.47 mW m^{-2}). Although the power density from MFC with 15 mg cm^{-2} of NAC-1 was slightly lower than that Pt/C, it was 48.5% higher under the same loading of b-AC.

The electrode potentials shown in Fig. 7c suggested the different activities of electrocatalysts. The anodic potentials of the MFCs were nearly identical because of the same electrode materials and inoculum used in the anodic chamber. This result suggested that cathodic performance played a critical role in power generation and energy recovery efficiency of MFCs. The cathodic performance was different among the tested electrocatalysts, and thus the energy recovery efficiency of MFCs, e.g., CE, was distinguishing by using different electrocatalysts. As shown in Fig. 7c, the cathodic potential at the open circuit was enhanced from 0.391 V (vs. SHE) for b-AC to 0.459 V (vs. SHE) for NAC-1, resulting in increased OCV.

To reach or exceed the power density of MFC with Pt/C as cathode electrocatalyst, AC-based catalyst loadings of more than 30 mg cm^{-2} on air-cathode were frequently required in previous studies [17, 20]. Many studies have reported high AC loadings but have not compared it with Pt/C. In the present work, a much lower loading of 15 mg cm^{-2} achieved the same level of power density as NAC-MFC to Pt/C-MFC possibly because of the high electrocatalytic activity of the NAC-1, thereby reducing the cost the cathode. Furthermore, a low loading reduced the thickness of the catalyst layer, which was beneficial for the mass transport of the air-cathode and decreases

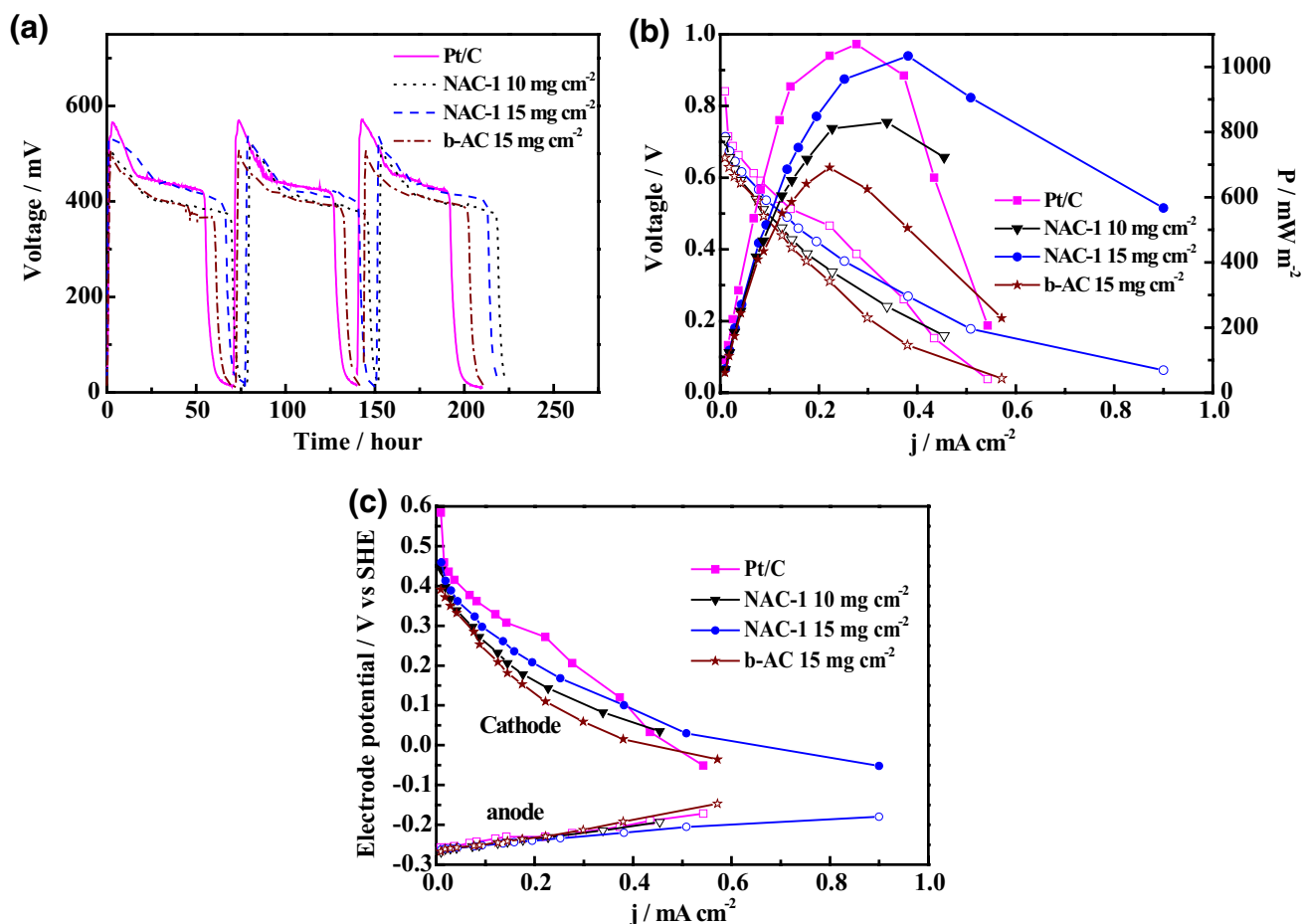


Fig. 7 The voltage–time profile (a), power density curves (b), and electrode potentials (c) of MFCs equipped with different cathode electrocatalysts

Table 3 Comparison of MFCs performance equipped with different cathode electrocatalysts

Samples	Maximum voltage (mV)	COD removal (%)	CE (%)	MPD (mW m^{-2})
b-AC (15 mg cm^{-2})	506.46 ± 2.36	91.26 ± 0.23	81.67 ± 1.26	690.86 ± 12.47
NAC-1 (10 mg cm^{-2})	514.17 ± 8.25	89.17 ± 3.71	93.43 ± 1.75	829.73 ± 9.31
NAC-1 (15 mg cm^{-2})	535.43 ± 1.53	90.22 ± 2.82	94.85 ± 2.29	1026.07 ± 10.83
Pt/C	568.85 ± 2.92	90.68 ± 1.09	86.17 ± 0.93	1065.33 ± 6.29

the resistance of MFCs. As shown in Fig. 7b, the current density responsible for MPD could be arranged as follows: 15 mg cm^{-2} of NAC-1 (0.38 mA m^{-2}) > 10 mg cm^{-2} of NAC-1 (0.33 mA m^{-2}) > Pt/C (0.27 mA m^{-2}) > 15 mg cm^{-2} of b-AC (0.22 mA m^{-2}), indicating the low internal resistance of MFCs equipped with NAC-1 as cathode electrocatalyst. A small amount of catalyst is desirable for the practical application of MFCs.

4 Conclusion

A macrocyclic compound, Pc, was selected as a nitrogen source for the synthesis of NAC. The prepared NAC displayed improved crystalline structure, high BET surface area and total pore volume, and an appropriate composition of micro- and mesopores. The elemental analysis

illustrated that the NAC also possessed an appropriate content of nitrogen and oxygen. As the mass ratio between AC and Pc was controlled at 1:1, the as-prepared NAC outperformed its counterparts in terms of ORR activity in neutral medium, including onset potential, electron transfer number, and ECSA. Owing to the high activity, a small amount of NAC with a loading of 15 mg cm^{-2} on the air-cathode was sufficient to achieve the level of MFC performance of a Pt/C catalyst specifically in terms of maximum power density and CE. The results indicated that NAC was a promising cathode electrocatalyst for MFC.

Acknowledgements This work was supported by the Natural Science Foundation of China (No. 51578526), the Chongqing Research Program of Basic Research and Frontier Technology (No. cstc2015jcyjBX0063), and by Natural Science Foundation of Chongqing (No. cstc2018jcyjAX0327), and the Youth Innovation Promotion Association of Chinese Academy of Sciences (No. 2016341).

References

- Logan BE, Hamelers B, Rozendal RA, Schrorder U, Keller J, Freguia S, Aelterman P, Verstraete W, Rabaey K (2006) Microbial fuel cells: methodology and technology. *Environ Sci Technol* 40:5181–5192. <https://doi.org/10.1021/es0605016>
- Logan BE, Rabaey K (2012) Conversion of wastes into bioelectricity and chemicals by using microbial electrochemical technologies. *Science* 337:686–690. <https://doi.org/10.1126/science.1217412>
- Santoro C, Arbizzani C, Erable B, Ieropoulos I (2017) Microbial fuel cells: from fundamentals to applications. A review. *J Power Sources* 356:225–244. <https://doi.org/10.1016/j.jpowsour.2017.03.109>
- Liew KB, Daud WRW, Ghasemi M, Leong JX, Lim SS, Ismail M (2014) Non-Pt catalyst as oxygen reduction reaction in microbial fuel cells: a review. *Int J Hydrogen Energy* 39:4870–4883. <https://doi.org/10.1016/j.ijhydene.2014.01.062>
- Yuan HY, He Z (2015) Graphene-modified electrodes for enhancing the performance of microbial fuel cells. *Nanoscale* 7:7022–7029. <https://doi.org/10.1039/c4nr05637j>
- Wang ZJ, Mahadevan GD, Wu YC, Zhao F (2017) Progress of air-breathing cathode in microbial fuel cells. *J Power Sources* 356:245–255. <https://doi.org/10.1016/j.jpowsour.2017.02.004>
- Liu Y, Liu H, Wang C, Hou SX, Yang N (2013) Sustainable energy recovery in wastewater treatment by microbial fuel cells: stable power generation with nitrogen-doped graphene cathode. *Environ Sci Technol* 47:13889–13895. <https://doi.org/10.1021/es4032216>
- Liu Y, Jin XJ, Tuo AX, Liu H (2016) Improved oxygen reduction reaction activity of three-dimensional porous N-doped graphene from a soft-template synthesis strategy in microbial fuel cells. *RSC Adv* 6:105211–105221. <https://doi.org/10.1039/c6ra23971d>
- You SJ, Gong XB, Wang W, Qi DP, Wang XH, Chen XD, Ren NQ (2016) Enhanced cathodic oxygen reduction and power production of microbial fuel cell based on noble-metal-free electrocatalyst derived from metal-organic frameworks. *Adv Energy Mater* 6:1501497. <https://doi.org/10.1002/aenm.201501497>
- Sun Y, Duan YQ, Hao L, Xing ZP, Dai Y, Li R, Zou JL (2016) Cornstalk-derived nitrogen-doped partly graphitized carbon as efficient metal-free catalyst for oxygen reduction reaction in microbial fuel cells. *ACS Appl Mater Interfaces* 8:25923–25932. <https://doi.org/10.1021/acsami.6b06895>
- Zhang F, Cheng SA, Pant D, Van Bogaert G, Logan BE (2009) Power generation using an activated carbon and metal mesh cathode in a microbial fuel cell. *Electrochem Commun* 11:2177–2179. <https://doi.org/10.1016/j.elecom.2009.09.024>
- Dong H, Yu HB, Wang X (2012) Catalysis kinetics and porous analysis of rolling activated carbon-PTFE air-cathode in microbial fuel cells. *Environ Sci Technol* 46:13009–13015. <https://doi.org/10.1021/es303619a>
- Li D, Qu YP, Liu J, He WH, Wang HM, Feng YJ (2014) Using ammonium bicarbonate as pore former in activated carbon catalyst layer to enhance performance of air cathode microbial fuel cell. *J Power Sources* 272:909–914. <https://doi.org/10.1016/j.jpowsour.2014.09.053>
- Ge Z, He Z (2015) An effective dipping method for coating activated carbon catalyst on the cathode electrodes of microbial fuel cells. *RSC Adv* 5:36933–36937. <https://doi.org/10.1039/c5ra05543a>
- Zhang XY, He WH, Yang WL, Liu J, Wang QY, Liang P, Huang X, Logan BE (2016) Diffusion layer characteristics for increasing the performance of activated carbon air cathodes in microbial fuel cells. *Environ Sci Water Res Technol* 2:266–273. <https://doi.org/10.1039/c5ew00245a>
- Dong H, Yu HB, Wang X, Zhou QX, Feng JL (2012) A novel structure of scalable air-cathode without Nafion and Pt by rolling activated carbon and PTFE as catalyst layer in microbial fuel cells. *Water Res* 46:5777–5787. <https://doi.org/10.1016/j.watres.2012.08.005>
- Watson VJ, Delgado CN, Logan BE (2013) Improvement of activated carbons as oxygen reduction catalysts in neutral solutions by ammonia gas treatment and their performance in microbial fuel cells. *J Power Sources* 242:756–761. <https://doi.org/10.1016/j.jpowsour.2013.05.135>
- Zhang F, Pant D, Logan BE (2011) Long-term performance of activated carbon air cathodes with different diffusion layer porosities in microbial fuel cells. *Biosens Bioelectron* 30:49–55. <https://doi.org/10.1016/j.bios.2011.08.025>
- Zhang XY, Pant D, Zhang F, Liu J, He WH, Logan BE (2014) Long-term performance of chemically and physically modified activated carbons in air cathodes of microbial fuel cells. *ChemElectroChem* 1:1859–1866. <https://doi.org/10.1002/celec.201402123>
- Zhang XY, Xia X, Ivanov I, Huang X, Logan BE (2014) Enhanced activated carbon cathode performance for microbial fuel cell by blending carbon black. *Environ Sci Technol* 48:2075–2081. <https://doi.org/10.1021/es405029y>
- Yang WL, Logan BE (2016) Immobilization of a metal–nitrogen–carbon catalyst on activated carbon with enhanced cathode performance in microbial fuel cells. *ChemSusChem* 9:2226–2232. <https://doi.org/10.1002/cssc.201600573>
- Zhang XY, Wang QY, Xia X, He WH, Huang X, Logan BE (2017) Addition of conductive particles to improve the performance of activated carbon air-cathodes in microbial fuel cells. *Environ Sci Water Res Technol* 3:806–810. <https://doi.org/10.1039/c7ew01018h>
- Li N, Liu YN, An JK, Feng CJ, Wang X (2014) Bifunctional quaternary ammonium compounds to inhibit biofilm growth and enhance performance for activated carbon air-cathode in microbial fuel cells. *J Power Sources* 272:895–899. <https://doi.org/10.1016/j.jpowsour.2014.09.008>
- Pu LT, Li KX, Chen ZH, Zhang P, Zhang X, Fu Z (2014) Silver electrodeposition on the activated carbon air cathode for performance improvement in microbial fuel cells. *J Power Sources* 268:476–481. <https://doi.org/10.1016/j.jpowsour.2014.06.071>
- Zhang X, Li KX, Yan PY, Liu ZQ, Pu LT (2015) N-type Cu₂O doped activated carbon as catalyst for improving power generation

- of air cathode microbial fuel cells. *Bioresour Technol* 187:299–304. <https://doi.org/10.1016/j.biortech.2015.03.131>
26. Huang QS, Zhou PJ, Yang H, Zhu LL, Wu HY (2017) CoO nanosheets in situ grown on nitrogen-doped activated carbon as an effective cathodic electrocatalyst for oxygen reduction reaction in microbial fuel cells. *Electrochim Acta* 232:339–347. <https://doi.org/10.1016/j.electacta.2017.02.163>
 27. Wang X, Gao NSJ, Zhou QX, Dong H, Yu HB, Feng YJ (2013) Acidic and alkaline pretreatments of activated carbon and their effects on the performance of air-cathodes in microbial fuel cells. *Bioresour Technol* 144:632–636. <https://doi.org/10.1016/j.biortech.2013.07.022>
 28. Chen ZH, Li KX, Zhang P, Pu LT, Zhang X, Fu Z (2015) The performance of activated carbon treated with H₃PO₄ at 80 °C in the air-cathode microbial fuel cell. *Chem Eng J* 259:820–826. <https://doi.org/10.1016/j.cej.2014.08.059>
 29. Wang Z, Liu Y, Li KX, Liu D, Yang TT, Wang JJ, Lu JF (2017) The influence and mechanism of different acid treatment to activated carbon used as air-breathing cathode catalyst of microbial fuel cell. *Electrochim Acta* 246:830–840. <https://doi.org/10.1016/j.electacta.2017.05.086>
 30. Watson VJ, Delgado CN, Logan BE (2013) Influence of chemical and physical properties of activated carbon powders on oxygen reduction and microbial fuel cell performance. *Environ Sci Technol* 47:6704–6710. <https://doi.org/10.1021/es401722j>
 31. Zhang B, Wen ZH, Ci SQ, Mao S, Chen JH, He Z (2014) Synthesizing nitrogen-doped activated carbon and probing its active sites for oxygen reduction reaction in microbial fuel cells. *ACS Appl Mater Interfaces* 6:7464–7470. <https://doi.org/10.1021/am5008547>
 32. Liu YT, Li KX, Liu Y, Pu LT, Chen ZH, Deng SG (2015) The high-performance and mechanism of P-doped activated carbon as a catalyst for air-cathode microbial fuel cells. *J Mater Chem A* 3:21149–21158. <https://doi.org/10.1039/c5ta04595a>
 33. Wang HM, Li D, Liu J, Liu LC, Zhou XT, Qu YP, Zhang J, Feng YJ (2016) Microwave-assisted synthesis of nitrogen-doped activated carbon as an oxygen reduction catalyst in microbial fuel cells. *RSC Adv* 6:90410–90416. <https://doi.org/10.1039/c6ra14387c>
 34. Xia X, Zhang F, Zhang XY, Liang P, Huang X, Logan BE (2013) Use of pyrolyzed iron ethylenediaminetetraacetic acid modified activated carbon as air-cathode catalyst in microbial fuel cells. *ACS Appl Mater Interfaces* 5:7862–7866. <https://doi.org/10.1021/am4018225>
 35. Pan YJ, Mo XP, Li KX, Pu LT, Liu D, Yang TT (2016) Iron-nitrogen-activated carbon as cathode catalyst to improve the power generation of single-chamber air-cathode microbial fuel cells. *Bioresour Technol* 206:285–289. <https://doi.org/10.1016/j.biortech.2016.01.112>
 36. Zitolo A, Goellner V, Armel V, Sougrati MT, Mineva T, Stievano L, Fonda E, Jaouen F (2015) Identification of catalytic sites for oxygen reduction in iron- and nitrogen-doped graphene materials. *Nat Mater* 14:937–942. <https://doi.org/10.1038/NMAT4367>
 37. Cao RG, Thapa R, Kim H, Xu XD, Kim MG, Li Q, Park N, Liu ML, Cho J (2013) Promotion of oxygen reduction by a bio-inspired tethered iron phthalocyanine carbon nanotube-based catalyst. *Nat Commun* 4:2076. <https://doi.org/10.1038/ncomms3076>
 38. de Oliveira MAC, Mecheri B, D'Epifanio A, Placidi E, Arciprete F, Valentini F, Perandini A, Valentini V, Licoccia S (2017) Graphene oxide nanoplateforms to enhance catalytic performance of iron phthalocyanine for oxygen reduction reaction in bioelectrochemical systems. *J Power Sources* 356:381–388. <https://doi.org/10.1016/j.jpowsour.2017.02.009>
 39. Santoro C, Gokhale R, Mecheri B, D'Epifanio A, Licoccia S, Serov A, Artyushkova K, Atanassov P (2017) Design of iron(II) phthalocyanine (FePc) derived oxygen reduction electrocatalysts for high power density microbial fuel cells. *ChemSusChem* 10:3243–3251. <https://doi.org/10.1002/cssc.201700851>
 40. Zhang ZP, Dou ML, Ji J, Wang F (2017) Phthalocyanine tethered iron phthalocyanine on graphitized carbon black as superior electrocatalyst for oxygen reduction reaction. *Nano Energy* 34:338–343. <https://doi.org/10.1016/j.nanoen.2017.02.042>
 41. Champavert J, Rejeb SB, Innocent C, Pontié M (2015) Microbial fuel cell based on Ni-tetra sulfonated phthalocyanine cathode and graphene modified bioanode. *J Electroanal Chem* 757:270–276. <https://doi.org/10.1016/j.jelechem.2015.09.012>
 42. Yang Y, Liu TY, Zhu X, Zhang F, Ye DD, Liao Q, Li Y (2016) Boosting power density of microbial fuel cells with 3d nitrogen-doped graphene aerogel electrode. *Adv Sci* 3:1600097. <https://doi.org/10.1002/advs.201600097>
 43. Jarzabek G, Borkowska Z (1997) On the real surface area of smooth solid electrodes. *Electrochim Acta* 42:2915–2918. [https://doi.org/10.1016/S0013-4686\(97\)00112-6](https://doi.org/10.1016/S0013-4686(97)00112-6)
 44. Konopka SJ, McDuffie B (1970) Diffusion coefficients of ferricyanide and ferrocyanide ions in aqueous media, using twin-electrode thin-layer electrochemistry. *Anal Chem* 42:741–746. <https://doi.org/10.1021/ac50160a042>
 45. Kim JR, Cheng SA, Oh SE, Logan BE (2007) Power generation using different cation, anion, and ultrafiltration membranes in microbial fuel cells. *Environ Sci Technol* 41:1004–1009. <https://doi.org/10.1021/es062202m>
 46. Zhang F, Saito T, Cheng SA, Hickner MA, Logan BE (2010) Microbial fuel cell cathodes with poly(dimethylsiloxane) diffusion layers constructed around stainless steel mesh current collectors. *Environ Sci Technol* 44:1490–1495. <https://doi.org/10.1021/es903009d>
 47. Lovley DR, Phillips EJP (1988) Novel mode of microbial energy metabolism: organic carbon oxidation coupled to dissimilatory reduction of iron or manganese. *Appl Environ Microbiol* 54:1472–1480
 48. Zhou XJ, Bai ZY, Wu MJ, Qiao JL, Chen ZW (2015) 3-Dimensional porous N-doped graphene foam as a non-precious catalyst for the oxygen reduction reaction. *J Mater Chem A* 3:3343–3350. <https://doi.org/10.1039/c4ta06538g>
 49. Lv K, Zhang H, Chen SL (2018) Nitrogen and phosphorus co-doped carbon modified activated carbon as an efficient oxygen reduction catalyst for microbial fuel cells. *RSC Adv* 8:848–855. <https://doi.org/10.1039/c7ra12907f>
 50. Jaouen F, Proietti E, Lefèvre M, Chenitz R, Dodelet JP, Wu G, Chung HT, Johnston CM, Zelenay P (2011) Recent advances in non-precious metal catalysis for oxygen-reduction reaction in polymer electrolyte fuel cells. *Energy Environ Sci* 4:114–130. <https://doi.org/10.1039/c0ee00011f>
 51. Videla AHAM, Zhang L, Kim J, Zeng J, Francia C, Zhang J, Specchia S (2013) Mesoporous carbons supported non-noble metal Fe-N(X) electrocatalysts for PEM fuel cell oxygen reduction reaction. *J Appl Electrochem* 43:159–169. <https://doi.org/10.1007/s10800-012-0497-y>
 52. Yang TT, Li KX, Pu LT, Liu ZQ, Ge BC, Pan YJ, Liu Y (2016) Hollow-spherical Co/N-C nanoparticle as an efficient electrocatalyst used in air cathode microbial fuel cell. *Biosens Bioelectron* 86:129–134. <https://doi.org/10.1016/j.bios.2016.06.032>
 53. Lai LF, Potts JR, Zhan D, Wang L, Poh CK, Tang CH, Gong H, Shen ZX, Lin JY, Ruoff RS (2012) Exploration of the active center structure of nitrogen-doped graphene-based catalysts for oxygen reduction reaction. *Energy Environ Sci* 5:7936–7942. <https://doi.org/10.1039/c2ee21802j>
 54. Zhang H, Yang JT, Hou HQ, Chen SL, Yao HM (2017) Nitrogen-doped carbon paper with 3d porous structure as a flexible free-standing anode for lithium-ion batteries. *Sci Rep* 7:7769. <https://doi.org/10.1038/s41598-017-07345-y>

55. Yu DS, Zhang Q, Dai LM (2010) Highly efficient metal-free growth of nitrogen-doped single-walled carbon nanotubes on plasma-etched substrates for oxygen reduction. *J Am Chem Soc* 132:15127–15129. <https://doi.org/10.1021/ja105617z>
56. Wang QY, Zhang XY, Lv RT, Chen X, Xue BR, Liang P, Huang X (2016) Binder-free nitrogen-doped graphene catalyst air-cathodes for microbial fuel cells. *J Mater Chem A* 4:12387–12391. <https://doi.org/10.1039/C6TA03642B>
57. Gong XB, You SJ, Wang XH, Zhang JN, Gan Y, Cui CW, Ren NQ (2014) Improved interfacial oxygen reduction by ethylenediamine tetraacetic acid in the cathode of microbial fuel cell. *Biosens Bioelectron* 58:272–275. <https://doi.org/10.1016/j.bios.2014.02.073>
58. Guo DH, Shibuya R, Akiba C, Saji S, Kondo T, Nakamura J (2016) Active sites of nitrogen-doped carbon materials for oxygen reduction reaction clarified using model catalysts. *Science* 351:361–365. <https://doi.org/10.1126/science.aad0832>
59. Zhou JH, Sui ZJ, Zhu J, Li P, Chen D, Dai YC, Yuan WK (2007) Characterization of surface oxygen complexes on carbon nanofibers by TPD, XPS and FT-IR. *Carbon* 45:785–796. <https://doi.org/10.1016/j.carbon.2006.11.019>
60. Liu Y, Jin XJ, Dionysiou DD, Liu H, Huang YM (2015) Homogeneous deposition-assisted synthesis of iron-nitrogen composites on graphene as highly efficient non-precious metal electrocatalysts for microbial fuel cell power generation. *J Power Sources* 278:773–781. <https://doi.org/10.1016/j.jpowsour.2014.12.134>
61. Du J, Mishra D, Ting JM (2013) Surface modified carbon cloth for use in electrochemical capacitor. *Appl Surf Sci* 285:483–489. <https://doi.org/10.1016/j.apsusc.2013.08.081>
62. Jung MJ, Jeong E, Lim JW, Lee SI, Lee YS (2011) Physico-chemical surface modification of activated carbon by oxyfluorination and its electrochemical characterization. *Colloid Surf A* 389:274–280. <https://doi.org/10.1016/j.colsurfa.2011.08.013>
63. Gong KP, Du F, Xia ZH, Durstock M, Dai LM (2009) Nitrogen-doped carbon nanotube arrays with high electrocatalytic activity for oxygen reduction. *Science* 323:760–764. <https://doi.org/10.1126/science.1168049>
64. Zhao X, Chu BT, Ballesteros B, Wang W, Johnston C, Sykes JM, Grant PS (2009) Spray deposition of steam treated and functionalized single-walled and multi-walled carbon nanotube films for supercapacitors. *Nanotechnology* 20:065605. <https://doi.org/10.1088/0957-4484/20/6/065605>
65. Pandolfo AG, Hollenkamp AF (2006) Carbon properties and their role in supercapacitors. *J Power Sources* 157:11–27. <https://doi.org/10.1016/j.jpowsour.2006.02.065>
66. Fu SF, Zhu CZ, Zhou YZ, Yang GH, Jeon JW, Lemmon J, Du D, Nune SK, Lin YH (2015) Metal-organic framework derived hierarchically porous nitrogen-doped carbon nanostructures as novel electrocatalyst for oxygen reduction reaction. *Electrochim Acta* 178:287–293. <https://doi.org/10.1016/j.electacta.2015.08.021>
67. Zhong RS, Qin YH, Niu DF, Tian JW, Zhang XS, Zhou XG, Sun SG, Yuan WK (2013) Effect of carbon nanofiber surface functional groups on oxygen reduction in alkaline solution. *J Power Sources* 225:192–199. <https://doi.org/10.1016/j.jpowsour.2012.10.043>
68. Li J, Song YJ, Zhang GX, Liu HY, Wang YR, Sun SH, Guo XW (2017) Pyrolysis of self-assembled iron porphyrin on carbon black as core/shell structured electrocatalysts for highly efficient oxygen reduction in both alkaline and acidic medium. *Adv Funct Mater* 27:1604356. <https://doi.org/10.1002/adfm.201604356>
69. Jaouen F, Dodelet JP (2009) O₂ reduction mechanism on non-noble metal catalysts for PEM fuel cells. Part I: experimental rates of O₂ electroreduction, H₂O₂ electroreduction, and H₂O₂ disproportionation. *J Phys Chem C* 113:15422–15432. <https://doi.org/10.1021/jp900837e>
70. Jaouen F (2009) O₂ reduction mechanism on non-noble metal catalysts for PEM fuel cells. Part II: a porous-electrode model to predict the quantity of H₂O₂ detected by rotating ring-disk electrode. *J Phys Chem C* 113:15433–15443. <https://doi.org/10.1021/jp900838x>

Affiliations

Yuan Liu^{1,2}  · Zhi-Mei Liu^{1,2}

✉ Yuan Liu
liuyuan@cigit.ac.cn

² Chongqing Institute of Green and Intelligent Technology,
Chinese Academy of Sciences, Chongqing 400714, China

¹ Key Laboratory of Reservoir Aquatic Environment, Chinese Academy of Sciences, Chongqing, China